Urban Water Journal

ISSN: 1573-062X (Print) 1744-9006 (Online) Journal homepage: www.tandfonline.com/journals/nurw20

Experimental measurements of biofilm thickness in drinking water pipes

Konstantinos Glynis , Mirjam Blokker , Zoran Kapelan & Dragan Savić

To cite this article: Konstantinos Glynis , Mirjam Blokker , Zoran Kapelan & Dragan Savić (16 Feb 2026): Experimental measurements of biofilm thickness in drinking water pipes, Urban Water Journal, DOI: 10.1080/1573062X.2026.2626794

To link to this article: https://doi.org/10.1080/1573062X.2026.2626794

Published online: 16 Feb 2026.

URBAN WATER JOURNAL
https://doi.org/10.1080/1573062X.2026.2626794

Taylor & Francis
Taylor & Francis Group

RESEARCH ARTICLE

OPEN ACCESS Check for updates

Experimental measurements of biofilm thickness in drinking water pipes

Konstantinos Glynis[a,b], Mirjam Blokker[a,b], Zoran Kapelan[a] and Dragan Savić[b,c]

[a]Department of Water Management, Delft University of Technology, Delft, Netherlands; [b]KWR Water Research Institute, Nieuwegein, Netherlands; [c]Centre for Water Systems, University of Exeter, Exeter, UK

ABSTRACT

Biofilms in drinking water distribution systems (DWDS) challenge water quality, infrastructure and public health. Current monitoring methods often disrupt biofilms or lack spatial coverage. This study explores two novel, non-intrusive techniques to measure biofilm thickness: one based on heat resistance, the other on changes in hydraulic residence time. Experiments were conducted in a lab-scale DWDS simulator replicating realistic pipe conditions. Both methods were evaluated against traditional destructive sampling to assess accuracy. Results show that the residence time method yields consistent, reliable estimates closely matching physical samples, while the heat resistance approach shows greater variability and requires refinement. Sensitivity analyses further demonstrate that the residence time method is more robust under varying operational conditions. These findings highlight its potential for field deployment, offering a scalable and minimally invasive solution for real-time biofilm monitoring. This advancement could support improved water quality management through targeted interventions in actual DWDS environments.

SYNOPSIS

This lab-based study tests new methods for measuring biofilm in drinking water pipes, providing foundational insights to support future field monitoring and improve water quality management practices.

ARTICLE HISTORY
Received 23 June 2025
Accepted 27 January 2026

KEYWORDS
Biofilm thickness; non-intrusive measurement; drinking water pipes; heat resistance; residence time

1. Introduction

Biofilms are structured communities of microorganisms that adhere to surfaces, encased in a self-produced extracellular matrix. In the context of drinking water distribution systems (DWDS), they are a pervasive and persistent concern, compromising water quality, system efficiency and public health (Liu et al. 2016; Moreno et al. 2024). It is estimated that more than 95% of the total biomass in DWDS is attached to the pipe wall, making biofilm the dominant microbial presence in these systems (Flemming, Percival, and Walker 2002). Their presence can lead to aesthetic issues, such as unpleasant taste, odour and discoloration, and more critically, the release of harmful substances and potential pathogens into the water (Fish, Osborn, and Boxall 2017; Husband et al. 2016; Vreeburg et al. 2009). Notable pathogenic bacteria like Escherichia coli, Pseudomonas aeruginosa and Legionella pneumophila have all been associated with biofilms in DWDS, highlighting the potential health risks posed by their unchecked growth (Flemming et al. 2016; Liu et al. 2016; van der Kooij and van der Wielen 2013).

Utilities typically rely on residual disinfectants such as chlorine to manage biofilms (Liu et al. 2016), but this approach is not without its limitations. Disinfection may not fully inhibit growth (Paquin et al. 1992) and can lead to the emergence of resistant microbial communities (Schwering et al. 2013). Moreover, chemical interactions with biofilms may release organic matter into the water and generate potentially harmful disinfection by-products (Fass et al. 2003; Singer 1994). Other strategies, such as hydraulic flushing, are effective but costly and operationally demanding (Lehtola et al. 2004; van der Kooij et al. 1999). While upstream nutrient limitation and bacterial load reduction are valuable proactive measures, they cannot eliminate biofilm formation altogether (Chen et al. 2013; Liu et al. 2016).

Future challenges such as rising temperatures and stricter regulatory standards are expected to exacerbate biofilm-related risks (Calero Preciado et al. 2022). Warmer distribution pipes provide more favourable conditions for both biofilm development and the proliferation of opportunistic pathogens (Calero Preciado et al. 2021; van der Wielen et al. 2023; Zlatanovic et al. 2017).

CONTACT Konstantinos Glynis kgglynis@tudelft.nl

As utilities face mounting pressures to ensure safe, high-quality water under increasingly constrained conditions (Delpla et al. 2009; Li et al. 2014), the need for reliable and practical biofilm monitoring becomes more urgent (Husband and Boxall 2011; Liu et al. 2016).

Understanding the state of the biofilm is a broad term encompassing a plethora of different features, each with different levels of maturity for field application. Researchers often focus on the microbiological composition and bio-activity of biofilms using gene- (Kalmbach, Manz, and Szewzyk 1997; Prest et al. 2016; Revetta et al. 2010) and protein-sequencing techniques (Afonso et al. 2024; Seneviratne et al. 2012). Knowing which bacterial phyla or species are present and/or active in the DWDS biofilms yields a huge breadth of information on the biological stability of the system and its potential for harbouring pathogens. This information is, however, limited to a specific location and time (Douterelo et al. 2016; Henne et al. 2012). Measuring the adenosine triphosphate (ATP) is also typical of microbiological approaches, as the detection of this protein is associated with bio-activity (Learbuch, Smidt, and Wielen 2021). Considering the naturally occurring biofilm heterogeneity, such sensitive information may change drastically across space and time (Neu et al. 2019). Significant research has also been performed on the physical attributes of biofilm. Biofilm coverage (Jungfer et al. 2013), thickness (Shen et al. 2016), roughness (Shen et al. 2015) and cohesiveness (Mathieu et al. 2014) have been studied among others.

Among the various measurable characteristics of biofilm, thickness stands out as a particularly informative and scalable parameter (Wagner and Horn 2017). It correlates strongly with biofilm growth and maturity, can influence hydraulic performance (Liu et al. 2016; Türetgen 2004) and is directly linked to bio-volume, which is straightforward to measure (Dreszer et al. 2013; Gomes, Simões, and Simões 2014). Microscopy-based techniques, including optical coherence tomography (OCT) and phase-contrast or fluorescence microscopy, are indeed well established for resolving biofilm structure. OCT has provided high-resolution, in situ imaging in flow-cell reactors equipped with transparent quartz windows (Zhao et al. 2023), while microfluidic systems have enabled detailed three-dimensional reconstructions of biofilms under controlled laboratory conditions (Liu et al. 2017).

However, these microscopy-based techniques rely on optically accessible, engineered geometries such as flat flow-cells or microfluidic chambers, which do not replicate cylindrical pipes or the hydraulic and material conditions of DWDS. They therefore yield localized measurements and cannot be applied in closed or buried pipe networks. Other non-invasive methods also remain limited to point-scale observations that do not capture biofilm heterogeneity or overcome the practical constraints of accessing real pipes (Bakke, Kommedal, and Kalvenes 2001; dos Santos and Livingston 1995; Maurício et al. 2013). These limitations highlight the need for non-intrusive techniques that work directly in full pipe geometries and provide spatially extensive information, as pursued in this study.

This study addresses this gap by experimentally evaluating two novel, non-intrusive methods for estimating biofilm thickness: one based on heat resistance and another on hydraulic residence time. Both methods are tested in a controlled laboratory setup designed to mimic key aspects of operational DWDS, providing a first step toward scalable and minimally invasive monitoring approaches. This work makes two main contributions. First, it presents and assesses two in-pipe biofilm thickness measurement techniques specifically developed for opaque, cylindrical pipes representative of real distribution systems. Second, it quantifies the sensitivity and operational limits of both methods under realistic hydraulic and thermal conditions, identifying the factors that most strongly influence measurement uncertainty. Together, these contributions support the development of more effective biofilm management strategies and support the transition toward proactive, data-driven DWDS operation.

2. Material and methods

2.1. Experimental facility and conditions

To measure the mean biofilm thickness $z_{biofilm}$ (μm) in drinking water pipes, we conducted experiments using a lab-scale pipe facility at KWR Water Research Institute (https://www.kwrwater.nl/en/), designed to replicate realistic DWDS conditions (Glynis et al. 2024), called 'Slimer'. The setup consists of a transparent RAUFILAM-E plasticized polyvinyl chloride (PVCp) pipe (Rehau AG, Muri bei Bern, Switzerland) with a length L_{pipe} of 50 m and an inner D_{in} and outer diameter D_{out} of 13.2 mm and 19.8 mm, respectively. This pipe material, despite being absent from real DWDS, was selected because of its high plasticizer content, which promotes biofilm growth (Learbuch, Smidt, and Wielen 2021). Its flexibility allows configuring the pipe in an upward helical arrangement to minimize the setup's physical footprint and increase the homogeneity of ambient conditions (see Figure 1).

To test the effect of biofouling on both the heat resistance alterations and hydraulic residence time, an array of sensors was installed in the 'Slimer'. We monitored temperature using three PT100 class

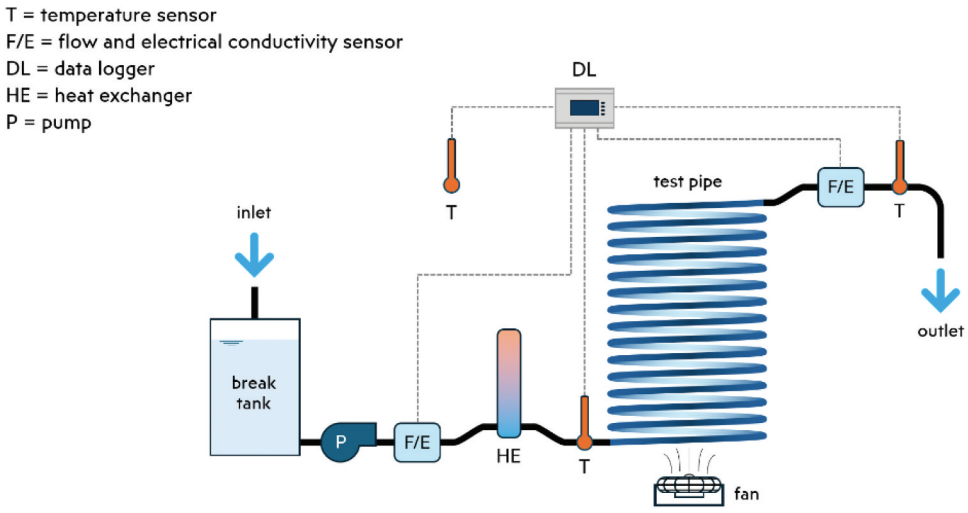

Figure 1. Slimer setup layout.

A temperature sensors (Labfacility Ltd, Bognor Regis, UK) at strategic points: one at the inlet, one at the outlet and one external near the pipe to monitor ambient conditions. These three sensors yielded T_{in}, T_{out} and T_{air} (all in °C), respectively. We monitored flow rate and electrical conductivity (EC) using two magnetic induction Picomag sensors (Endress+Hauser AG, Reinach, Switzerland) at both ends of the pipe. The upstream sensor yielded EC_{in} (µS/cm), and the downstream sensor provided EC_{out} (µS/cm), and Q (l/h).

We placed the setup in a dark, temperature-controlled room to maintain stable environmental conditions and eliminate light exposure. The water used in the experiments was unchlorinated, following common practice in the Netherlands (van der Kooij et al. 1999), and was supplied by the local water utility. Appendix A provides details on the basic physicochemical properties of the water used. The system operated in a pass-through mode without recirculation, with a break tank at the inlet for safety. Furthermore, we installed a DOMO floor fan Ø 40 cm (Linea 2000 BV, Herentals, Belgium) at the ground level of the helical pipe axis to minimize air conditioner-induced variations in the temperature and ensure a consistent convective heat transfer effect from the air to the pipe.

Biofilm was developed from 18 February to 17 December 2024. During this period, the system operated under three conditioning flow-rate regimes (Q_{cond}): 50 L/h for the first 72 days, 200 L/h for the following 59 days and 400 L/h for the final 135 days. Previous work demonstrates that higher or varying shear stress conditions lead to biofilms that are more compact, cohesive and adapted to hydraulic loading (Fish, Osborn, and Boxall 2017; Tsagkari et al. 2022). Accordingly, by increasing Q_{cond} over time we attempted to mimic realistic DWDS shear conditions and avoid formation of thick, loosely attached low-shear biofilms, thereby fostering a shear-conditioned structure more representative of full-scale systems. Thickness measurements were performed at testing flow rates (Q_{test}) equal to or lower than Q_{cond} to avoid exposing the biofilm to excessive shear. In this framework, Q_{test} defines the instantaneous hydraulic conditions during measurement, while Q_{cond} represents the long-term shear environment under which the biofilm developed. Additional time outside these regimes was used for system conditioning and sensor calibration. Ambient temperatures were consistently maintained between 24°C and 28°C. Reynolds numbers varied from 540 to 10,700. Hydraulic regime characterization accounted for temperature-dependent water viscosity, which ranged from 1.31 to 1.11 mPa·s as inlet temperatures varied between 12°C and 16°C (Çengel 2002). This affected Reynolds numbers slightly, but flow regimes remained consistent across experiments. Further details on the experimental conditions are provided in Appendix D.

Following the 10-month conditioning period and the presence of mature biofilm, we removed the biofilm deposits by pigging. We performed this using a sterilized custom-built pig, made of four silicon rings attached to a stainless steel core and collected the water and biofilm aggregate into a sterilized 20 l beaker for further microbiological analysis. The latter validated the presence of biofilm in the pipe, as is explained in Biofilm presence validation. The cleaning of the pipe allowed us to measure the difference between biofouled and clean conditions, as described in Biofilm thickness through heat resistance measurements and Biofilm thickness through residence time measurements.

2.2. Biofilm presence validation

We validated the presence of biofilm in the pipe through two independent measurements: (i) quantification of biofilm volume and (ii) assessment of biological activity via ATP (van der Wielen and van der Kooij 2010).

Biofilm deposits were removed from the pipe by pigging and collected in a sterilized container. The mixture was divided into 1 L subsamples and centrifuged at 3000 G for 10 min following CEN-EN 16,421:2014 (CEN 2014). This procedure separated the solid biofilm fraction from the bulk water, enabling measurement of the dehydrated biofilm volume. To compare this with calculated thickness values, the total solid volume was divided by the internal pipe surface area, yielding an average biofilm thickness under the assumption of uniform coverage (Eq. 1).

$$z_{biofilm} = \frac{V_{biofilm}}{\pi \cdot D_{in} \cdot L_{pipe}} \tag{1}$$

Bioactivity was quantified using a luciferin – luciferase ATP assay (CEN 2014). After adding a nucleotide-releasing buffer, light emission was measured with a Celsis Advance II luminometer (Celsis International B. V., Maastricht-Airport, The Netherlands) and converted to ATP concentrations using calibration curves. Biofilm ATP was expressed as pg cm^{-2}, while water ATP (ng L^{-1}) was converted to the same units for comparison.

We acknowledge that this biovolume method introduces uncertainty. Detachment and centrifugation may remove or dehydrate extracellular polymeric substances (EPS), causing the measured volume to underestimate the true hydrated biovolume. The calculation also assumes uniform thickness despite known spatial heterogeneity of DWDS biofilms. Thus, the values represent conservative, pipe-averaged estimates rather than absolute volumes; a consideration that appears reasonable given the relatively uniform biofilm coverage observed in our setup (see Appendix G). Nevertheless, the approach provides internally consistent indicators of biofilm accumulation suitable for validating biofilm presence.

The overview of the parameters used in the experiments is provided in Table 1.

2.3. Biofilm thickness through heat resistance measurements

Our setup allows for a precise measurement of the heat resistance R of drinking water pipes by ensuring stable environmental conditions and well-defined pipe properties. In the setup, as cold water travels through the pipe, it absorbs thermal energy E_{th}, leading to a temperature increase between the inlet T_{in} and outlet T_{out}. Given a constant mass flow rate m (kg/s) and a known specific heat of water $C_{p,water}$, (J/kg·K) the energy conservation equation for steady fluid flow in a tube applies (Çengel 2002) is as follows:

$$\frac{dE_{th}}{dt} = m \cdot C_{p,water} \cdot (T_{out} - T_{in}) \tag{2}$$

The thermal energy absorbed by the water flow must pass from the air through the pipe wall (and biofilm, if present) and into the water. The temperature dynamics in pipes have been previously studied (Çengel 2002) and assuming that the outer wall temperature is equal to the air temperature, they are characterized as follows:

$$\frac{dT_{water}}{dt} = \frac{2}{\rho_{water} \cdot r \cdot C_{p,water}} (T_{air} - T_{water}) \tag{3}$$

where T_{water} is the water temperature, T_{air} is the air temperature, ρ_{water} (kg/m^3) is the water density and r is the pipe radius ($r = 0.5D_{in}$). Assuming a uniform water temperature at the cross-section level, the integration across the entire pipe length yields the total heat resistance R_{total} (°C/W) provided in the following equation:

$$R_{total} = \frac{1}{m \cdot C_{p,water} \cdot ln\left(\frac{T_{air} - T_{out}}{T_{air} - T_{in}}\right)} \tag{4}$$

R_{total} can be decomposed into the sum of the internal heat resistance R_{int}, which is influenced by hydraulics and more specifically the boundary layer, the heat resistance of the pipe material itself R_{pipe}, the

Table 1. Overview of the experiment parameters.

Parameter	Symbol	Value	Unit	Source
Water inlet temperature	T_{in}	[12, 16]	°C	Measured
Water outlet temperature	T_{out}	[13, 22]	°C	Measured
Ambient air temperature	T_{air}	[24, 28]	°C	Measured
Flow rate	Q	[20, 400]	L/h	Measured
Density of water at 15°C	ρ_{water}	999.1	kg/m^3	Çengel (2002)
Specific heat of water at 15°C	$C_{p,water}$	4190	J/kg/°C	Çengel (2002)
Thermal conductivity of water at 15°C	k_{water}	0.58	W/m/°C	Çengel (2002)
Thermal conductivity of PVC at 15°C	k_{pipe}	0.15	W/m/°C	Anderson (1966)
Pipe length	L_{pipe}	50	m	Measured
Inner pipe diameter	D_{in}	13.2	mm	Measured
Outer pipe diameter	D_{out}	19.8	mm	Measured

external heat resistance R_{ext}, which depends on the environmental conditions, and in the case of a biofouled pipe, the resistance of the biofilm itself $R_{biofilm}$, as described in the following equation (Çengel 2002):

$$R_{total} = R_{int} + R_{biofilm} + R_{pipe} + R_{ext} \quad (5)$$

To determine the internal heat resistance, we use the hydraulic conditions within the pipe, particularly focusing on the ratio of total heat transfer to conductive heat transfer at the boundary, represented by the Nusselt number Nu_{water}. This relationship is expressed as follows:

$$R_{int} = \frac{1}{\frac{k_{water} \cdot Nu_{water}}{D_{in}} \left(\pi \cdot D_{in} \cdot L_{pipe}\right)} \quad (6)$$

where the water's thermal conductivity k_{water} (W/m·K), D_{in} and L_{pipe} are known, and Nu is calculated from the Dittus–Boelter correlation (Çengel 2002). The pipe heat resistance is therefore calculated from the geometry of the pipe (D_{in}, D_{out}, L_{pipe}) and the pipe material thermal conductivity k_{pipe} (W/m·K), as is provided as follows:

$$R_{pipe} = \frac{ln(D_{out}/D_{in})}{2 \cdot \pi \cdot k_{pipe} \cdot L_{pipe}} \quad (7)$$

The external component of heat resistance depends on the external heat transfer coefficient h_{ext} (W/m^2·K). This coefficient is a function of the thermal conductivity of air k_{air} (W/m·K), D_{out} and the Nusselt number of the air flow around the pipe Nu_{air}, which itself depends on the airflow (Çengel and Ghajar 2015).

$$R_{ext} = \frac{1}{\pi \cdot D_{out} \cdot L_{pipe} \cdot h_{ext}} = \frac{1}{\pi \cdot L_{pipe} \cdot k_{air} \cdot Nu_{air}} \quad (8)$$

Calculating this external component of heat resistance is a challenging, and often impractical task, because knowledge of the airflow convection and conduction dynamics is required. Therefore, we choose to not calculate it using Eq. (8), but rather derive it by subtracting the sum of R_{int} and R_{pipe}, under biofilm-free conditions from the measurable $R_{total,t=0}$. Assuming steady environmental conditions, the external component remains unchanged over time, i.e. $R_{ext,t=0} = R_{ext}$, and we attribute any change in R_{total} to biofilm-induced heat resistance $R_{biofilm}$. Assumptions about the air flow, however, seem to yield R_{ext} values the same order of magnitude as the calculated ones. More details about this are provided in Appendix B.

To extract the $z_{biofilm}$, we leverage the observation that biofilm comprises mostly water (Flemming and Wingender 2010). By assuming a homogeneous biofilm density with a thermal conductivity equal to that of water k_{water}, we calculate $z_{biofilm}$ as the thickness of the layer required to induce $R_{biofilm}$. This is described as follows:

$$z_{biofilm} = \pi \cdot D_{in} \cdot L_{pipe} \cdot k_{water} \cdot R_{biofilm} \quad (9)$$

It is important to note that the heat resistance measurements in this study were performed in new, non-corroded pipes under controlled laboratory conditions, minimizing interference from pipe aging. However, heat resistance estimates can also be influenced by environmental and water-quality factors. Variations in natural organic matter, dissolved solids or particulates may affect thermal properties and reduce the observable temperature difference between inlet and outlet, introducing additional uncertainty in the calibration of R_{total} and potentially masking the biofilm influence. Although the water used here was biologically stable and low in nutrients (Table A.1), such effects may be more pronounced in real DWDS. Field application of the heat resistance method would therefore require careful calibration under variable water-quality conditions to avoid systematic biases.

2.4. Biofilm thickness through residence time measurements

Measuring the hydraulic residence time t_{res} requires tracer experiments based on changes in electrical conductivity (EC). The baseline EC of water in the Slimer setup is 284 ± 2 µS/cm, well below the 500 µS/cm threshold typically considered soft water. By introducing a low concentration of sodium chloride (NaCl), specifically, 180 mg dissolved in 2 L of water added to the upstream break tank, we increase the EC without exceeding this threshold. This minimal increase preserves water chemical stability and biofilm integrity. Moreover, the use of low-concentration NaCl as a conductivity tracer is feasible in actual drinking water distribution systems, providing a practical and non-disruptive method for monitoring hydraulic residence time under real-world conditions.

As the NaCl solution enters the flow, a pulse of increased salinity propagates through the system, producing a transient rise in EC. This pulse is detected by the upstream (EC_{in}) and downstream (EC_{out}) sensors, appearing as an EC peak against the background level of 284 µS/cm. Depending on flow conditions and salt concentration, the peak typically reaches approximately 450 µS/cm. From the EC time series at each sensor, we extract the time at which the pulse passes through.

To isolate the pulse, we set a threshold at 289 µS/cm corresponding to background EC plus a 95% confidence interval. This prevents the inclusion of natural EC fluctuations unrelated to the pulse. From the isolated pulse, we compute the 25th, 50th and 75th percentile EC values.

We also extract the mean weighted by the EC values exceeding the threshold, representing the 'center of gravity' of the pulse. Recognizing the pulse's irregular shape, we define three time instance definitions to represent its passage at each sensor (i = 1 for EC_{in}, i = 2 for EC_{out}). These are as follows: $t_{i,1}$ corresponding to the 50th percentile (median) time, $t_{i,2}$ to the mean of the 25th and 75th percentile times and $t_{i,3}$ to the exceedance-weighted mean time of the pulse. Residence times $t_{res,j}$ are calculated as the time difference between the EC peaks detected in EC_{in} and EC_{out} at times $t_{1,j}$ and $t_{2,j}$ respectively, where $j = 1, 2, 3$ represents the corresponding time instance definition. The resulting residence time $t_{res,j}$ is the difference of the arrival times $t_{1,j}$ and $t_{2,j}$ at EC_{in} and EC_{out}, respectively, as follows:

$$t_{res,j} = t_{2,j} - t_{1,j} \tag{10}$$

where $t_{1,j}$ and $t_{2,j}$ is the travel time of the pulse until EC_{in} and EC_{out} accordingly.

By maintaining a constant flow rate Q, the presence of biofilm volume constricts the flow of water leading to an increase in water velocity and a reduction in $t_{res,j}$. Let $t_{res,clean,j}$ and $t_{res,biofilm,j}$, the hydraulic residence time in a clean and biofouled pipe, respectively, for the time instance definition j. Then, $z_{biofilm,j}$ is calculated as the thickness of the layer required to constrict the flow and lead to a decrease in residence time from $t_{res,clean,j}$ to $t_{res,biofilm,j}$, as is described here:

$$z_{biofilm,j} = \frac{D_{in}}{2}\left(1 - \sqrt{\frac{t_{res,biofilm,j}}{t_{res,clean,j}}}\right) \tag{11}$$

An explanation of the derivation of Eq. (11) is provided in Appendix C. The final $z_{biofilm}$ for each flow rate is calculated as the mean of the three $z_{biofilm,j}$ corresponding to the three different time instance definitions. The population of $z_{biofilm,j}$ values is used to also calculate the standard deviation of the biofilm thickness measurements.

We acknowledge that in real DWDS, hydraulic residence time is affected by a number of different dynamic factors and the assumption of a constant flow rate Q is improbable. However, in this study, a closed and controlled laboratory setup was used to isolate the impact of biofilm growth on residence time, serving as a proof of concept for further validation under realistic conditions.

2.5. Sensitivity analysis

To assess the robustness of the two biofilm-thickness estimation methods, we evaluated how measurement uncertainties propagate into the calculated heat resistance and residence time results. For the heat resistance method, uncertainty in R_{total} was quantified using standard Gaussian error propagation applied to the measured inlet, outlet and air temperatures and to the flow-rate – derived mass flux. Partial derivatives of R_{total} with respect to these variables were used to obtain the combined uncertainty. The detailed derivation and numerical substitutions for each flow rate are provided in Supporting Information (Appendix D).

Using representative experimental values, the resulting biofilm thickness uncertainties ranged from 179 µm at 200 L/h to 962 µm at 50 L/h, highlighting the varying degree of sensitivity of this method; high sensitivity at longer residence times (or low flow conditions), lower at shorter residence times (or high flow conditions).

For the residence time method, uncertainty was assessed using the variation among the three time-instance definitions extracted from the EC pulse at each sensor. Error propagation applied to Eq. (11) yields the final thickness uncertainty, with full derivation provided in Appendix D. At 200 L/h, this resulted in an uncertainty of 14 µm, approximately an order of magnitude lower than that of the heat resistance method. The superior sensitivity of the residence time method reflects the stability of EC measurements relative to temperature-based estimates of heat transfer.

3. Results and discussion

3.1. Biofilm thickness from heat resistance and hydraulic residence time methods

The heat resistance method results in Table 2 reveal that the measured biofilm thickness $z_{biofilm}$ varies across different flow rates and regimes. At 200 l/h (Re = 5,360), the thickness could not be determined, as R_{tot} unexpectedly decreased in the presence of biofilm. This would result in a negative $z_{biofilm}$, which is physically impossible. This

Table 2. Biofilm thickness $z_{biofilm}$ with 68% confidence interval measured with the heat transfer method.

Q_{test} (l/h)	u_{mean} (m/s)	Re (–)	R_{int} (°C/W)	R_{pipe} (°C/W)	R_{ext} (°C/W)	$R_{tot,biofilm}$ (°C/W)	$R_{tot,clean}$ (°C/W)	$z_{biofilm}$ (µm)
200	0.36	5360	0.002	0.0086	0.0118	0.0211	0.0212	–
150	0.27	4020	(turbulent)/0.0030 (laminar)			0.0215	0.0215	**8 ± 247**
100	0.18	2680				0.0219	0.0216	**290 ± 394**
50	0.09	1340				0.0221	0.0217	**588 ± 962**

finding suggests either that the heat resistance of the clean pipe exceeds that of the biofouled pipe or that the equation parameters used are inaccurate. The latter may be attributed to the assumption that Re = 5,360 corresponds to turbulent flow, leading to $Nu_{water} = 39.82$ and $R_{int} = 0.0003$ °C/W. However, if this assumption is incorrect and the flow is actually laminar, then Nu_{water} would be 3.66 resulting in $R_{int} = 0.0030$ °C/W. If biofilm presence disrupts the flow sufficiently to induce a transition from turbulence to laminar conditions, the resulting discrepancy of 0.0027 °C/W in R_{int} would more than account for the observed reduction in $R_{tot,biofilm}$ compared to $R_{tot,clean}$.

At lower flow rates of 150 and 100 l/h the measured biofilm thickness $z_{biofilm}$ surpasses the zero threshold, reaching 8 µm and 290 µm, respectively. However, the associated uncertainty remains substantial, at 247 µm and 394 µm, even surpassing the average values. This trend becomes even more pronounced at the lowest flow rate of 50 l/h, where $z_{biofilm}$ reaches 588 µm, yet the high uncertainty of 962 µm underscores the challenge of obtaining precise measurements under low-flow conditions.

The progressively increasing values of $z_{biofilm}$ measured at lower lower flow rates may be explained by three potential reasons. Firstly, at lower flow rates water experiences longer residence times, which allows greater temperature difference between the bulk water inside the pipe and the environment outside of the pipe to be developed. This increases the sensitivity of the measurements, as this is reflected in the coefficient of variation, i.e. the standard deviation-to-mean ratio. Secondly, at low flow rates where we have laminar conditions, the contribution of the boundary layer possibly transcends what the equations account for in a clean pipe. That is because the inhomogeneous biofilm layer increases hydraulic resistance and pushes the boundary layer to increase. Thirdly, at lower flow rates, the shear stress that exerts pressure on the biofilm is reduced, allowing for 'fluffier' biofilm. This increase in its effective thickness entraps stagnated water in between its 'fluffy' protrusions, effectively increasing the total heat resistance biofilm contributes to the system.

The residence time method yielded biofilm thickness $z_{biofilm}$ values approximately 10 times smaller than those obtained using the heat resistance method (see Table 3).

Several observations arise from the results shown in Table 3. Firstly, all measurements produced positive $z_{biofilm}$ values, confirming, as expected, an increase in residence time due to biofilm removal across the flow rate spectrum. Secondly, the residence time method exhibits significantly lower uncertainty compared to the heat resistance method, reflecting differences in the stability of the underlying measurements. The residence time method relies on electrical conductivity, a parameter that remains relatively stable in drinking water because it primarily reflects source-water composition and is minimally influenced by biological activity in distribution, at least in the integral DWDS of the Netherlands. In contrast, the heat resistance method depends on detecting minute temperature differences, and temperature is inherently dynamic, influenced by thermal exchange with the environment, sensor placement and fluctuating hydraulic conditions. These factors lead to markedly higher variability in the heat resistance estimates.

When the two methods are compared directly, an approximate tenfold discrepancy in $\boldsymbol{z_{biofilm}}$ becomes apparent. This mismatch arises from fundamental methodological differences. The heat resistance method is built on a simplified thermal model that assumes the biofilm behaves as a homogeneous layer with water-like thermal conductivity, whereas real biofilms comprise cells, EPS, voids and trapped water, resulting in different and potentially heterogeneous thermal properties. Additionally, because the method infers biofilm resistance from minimal temperature differences between inlet and outlet, it is highly sensitive to measurement noise, assumptions about the flow regime and external convection effects. These compounding uncertainties tend to inflate the calculated thickness. In contrast, the residence time method responds mainly to geometric constriction of the pipe's cross-section and relies on stable EC measurements, yielding substantially lower uncertainty. The stronger agreement between the residence time results and the destructively measured biofilm thickness (see Section 3.2) further supports the interpretation that, under the controlled conditions of this study, the heat resistance method systematically overestimates biofilm thickness.

Table 3. Biofilm thickness $z_{biofilm}$ with 68% confidence interval measured with the residence time method.

Q_{test} (l/h)	u_{mean} (m/s)	Re (–)	$\bar{t}_{res,biofilm}$ (s)	$\bar{t}_{res,clean}$ (s)	$z_{biofilm}$ (µm)
200	0.36	5360	135.6	137.0	**33 ± 6**
150	0.27	4020	181.6	182.0	**8 ± 3**
100	0.18	2680	270.3	272.8	**31 ± 4**
50	0.09	1340	531.2	543.4	**75 ± 4**

Taken together, these observations demonstrate that the two methods respond to fundamentally different physical mechanisms, thermal exchange versus hydraulic constriction, which explains their divergent sensitivities and operational limits. This distinction is essential for selecting appropriate biofilm thickness monitoring strategies in practice, as the reliability of each method depends strongly on flow regime, pipe material and the expected magnitude of biofilm accumulation.

3.2. Biofilm presence

At the end of the biofilm growth phase, pigging and centrifugation yielded a solid biofilm volume of 32 mL, corresponding to a minimum equivalent thickness of 15.5 µm based on Eq. (1). This value reflects the dehydrated state of the biomass and assumes complete removal without residuals. Despite these conservative assumptions, the destructive thickness aligns well with the residence time estimates at 200 and 150 L/h (33 ± 18 and 8 ± 9 µm) and is lower than the values at 100 and 50 L/h (31 ± 12 and 75 ± 12 µm). These deviations at low flow rates likely arise from the increasing porosity and decompression of biofilm under laminar conditions, which reduces apparent cross-sectional area and enhances the residence time signal (S. Liu et al. 2016).

The destructive measurement differs substantially from the heat resistance thicknesses reported in Table 2. As discussed in Section 3.1, the heat resistance method tends to overestimate $z_{biofilm}$ under the conditions of this study. The destructive value therefore provides a useful reference point, indicating that the residence time method offers a closer representation of the actual biofilm accumulation.

ATP analysis of the centrifuged material yielded a pipe-averaged concentration of 7200 ± 620 pg ATP/cm^2, confirming high bioactivity. This likely reflects the biofilm-promoting characteristics of the PVPp pipe's plasticizer content and suggests the biofilm was sufficiently mature for comparative validation.

Figure 2 summarizes the destructive measurement alongside the two non-intrusive methods. The destructive benchmark supports the interpretation that the residence time method provides realistic and flow-consistent thickness estimates, whereas the heat resistance values should be interpreted cautiously and mainly as qualitative indicators under controlled temperature conditions.

3.3. Reproducibility of the methods

The derivation of biofilm thickness from heat resistance measurements involves several simplifying assumptions to facilitate analytical calculations. Although these assumptions do not fully capture the complexities of real-world drinking water distribution systems, they establish a necessary baseline to evaluate the feasibility and potential of this non-intrusive method. We acknowledge that further refinement and validation at pilot-scale are essential to account for additional factors such as variable flow regimes, pipe aging and environmental influences.

Regarding the reproducibility of the heat resistance method, it is important to assess whether the results obtained in the controlled Slimer laboratory setup can be replicated with comparable accuracy in other settings, including pilot distribution networks. To explore this, we reformulate Eq. (3), which describes how water temperature changes as the water transits the water pipe. By integrating the equation with respect to the water temperature and calculating the outlet temperature T_{out} as a function of the inlet and air temperature T_{in} and T_{air}, respectively, we get:

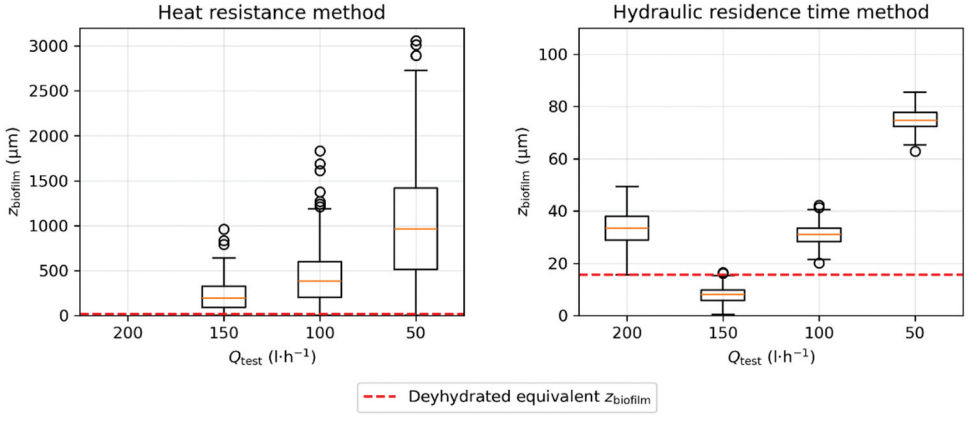

Figure 2. Biofilm thickness estimates from the heat resistance method, residence time method and destructive measurement.

$$T_{out} = T_{air} - (T_{air} - T_{in})e^{-\frac{\pi \cdot L \cdot D_{in}}{\dot{m} \cdot c_{p,water} \cdot R_{total}}} \quad (12)$$

Eq. (12) describes an asymptotic convergence of the water temperature to the air temperature for a certain R_{total}. Any change in R_{total}, e.g. by 10% as depicted in Figure 2 below, will result in a different T_{out} at the pipe outlet. The discrepancy of T_{out} we name discreteness. If we depict the operating setpoint of, e.g. 200 l/h for the biofouled conditions observed on 16 December 2024, in a T_{water}-t_{res} plane, we get Figure 3.

As shown in Figure 3, the vertical displacement in water temperature between original and altered heat resistance conditions, i.e. the discreteness in heat resistance changes, is greatest at a residence time (t_{res}) of approximately 800 s, where the dark and light blue lines diverge the most.

For L_{pipe} of 50 m and D_{in} of 13.2 mm, $t_{res} = 123$ s. At this level, variations in R_{total} influence the discreteness of detectable T_out changes. For instance, a ± 10% change (light blue in Figure 2) results in a T_{out} shift of only ±0.21°C. If the pipe were 300 m long ($t_{res} = 739$ s), the same R_{total} change would yield ±0.47°C in T_{out}. However, with constant mass flux, $\frac{\partial z_{biofilm}}{\partial R_{total}}$, linearly dependent on L_{pipe}, would increase proportionally (see Section 2.5), significantly raising $\sigma_{z_{biofilm}}$. Thus, for longer pipes, higher flow rates are needed to reduce the partial differentials in Eqs. (D.1)–(D.4) (see Appendix D) and limit $\sigma_{z_{biofilm}}$.

Consider a case with a pipe 100 times wider (D_{in} = 132.0 mm), carrying 100 times more flow (Q = 20,000 l/h) over a length four times greater (L_{pipe} = 200 m). The residence time becomes $t_{res} = 493$ s. While discreteness drops to ±0.11°C, the increased mass flow and pipe length result in $\sigma_{z_{biofilm}} = 40$ µm. This demonstrates improved sensitivity of the heat resistance method for longer, high-flow pipes, conditions more representative of real DWDS.

Assuming the biofilm has the same thermal conductivity as water (k_{water}), its impact on R_{total} is minor. In a 13.2 mm pipe (as in 'Slimer'), a 100 µm thick biofilm raises R_{total} by just 8.3×10^{-5} °C/W (a 0.35% change), causing negligible T_{out} variation. Figure 4 illustrates this biofilm's effect on ΔT_{out} across four pipe diameters and two materials (plasticized and unplasticized PVC), assuming constant Reynolds number.

As shown, the maximum observed ΔT_{out} remains below the 0.02°C threshold, even for the smallest pipe diameter investigated, i.e. the one used in Slimer. This highlights the inability of the sensors to reliably detect changes in outlet temperature, even under optimal pipe dimensions. Thus, refining this method is crucial, particularly by better characterizing the thermal properties of biofilm and their influence on the detectability of biofilm-induced changes in heat resistance.

Regarding the hydraulic residence time method, its reproducibility in real-world DWDS depends on the sampling frequency of the EC meters used and the minimum Δt_{res} required for sufficient accuracy. Assuming similar sensors recording at 10 Hz, and considering a permissible residence time discplacement of at least 2 s (equivalent to 20 recorded entries), we examine the operational conditions necessary to achieve these measurements.

For pipe sections of similar length (L_{pipe} = 50 m), a Δt_{res} = 2 sec is measured at different flow rates for larger pipe diameters D_{in} ranging from 13.2 mm up to 200 mm for a maximum flow rate as is shown in Figure 5:

Figure 5 shows that, depending on the biofilm thickness $z_{biofilm}$, the larger the inner pipe diameter in place D_{in}, the higher the flow rate required to measure this

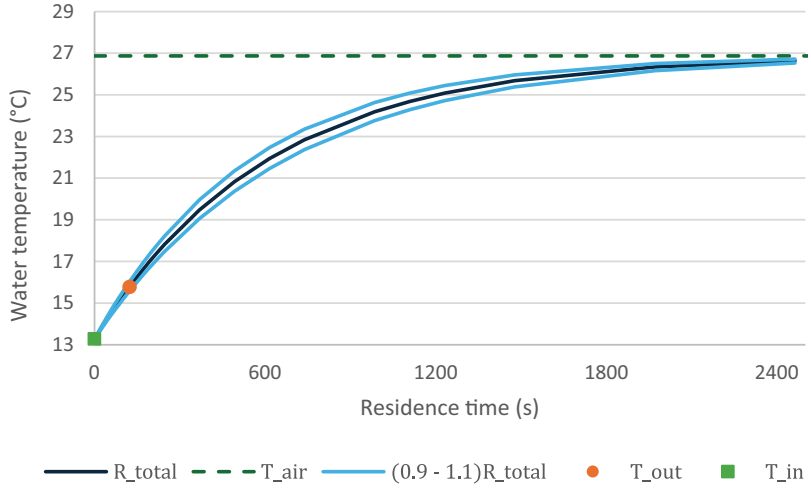

Figure 3. Water temperature in Slimer setup for 200 l/h.

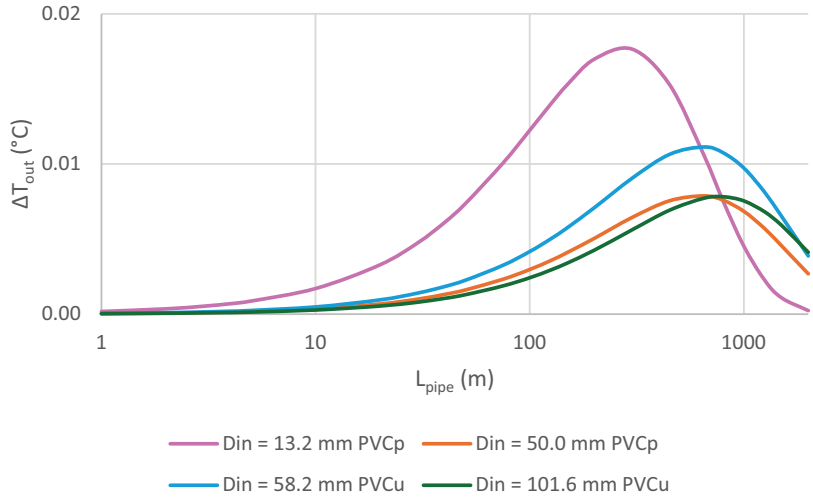

Figure 4. Theoretical variation in measured outlet temperature along the pipe length for different pipe diameters and materials, assuming identical biofilm thickness (100 µm) and Reynolds number (5360).

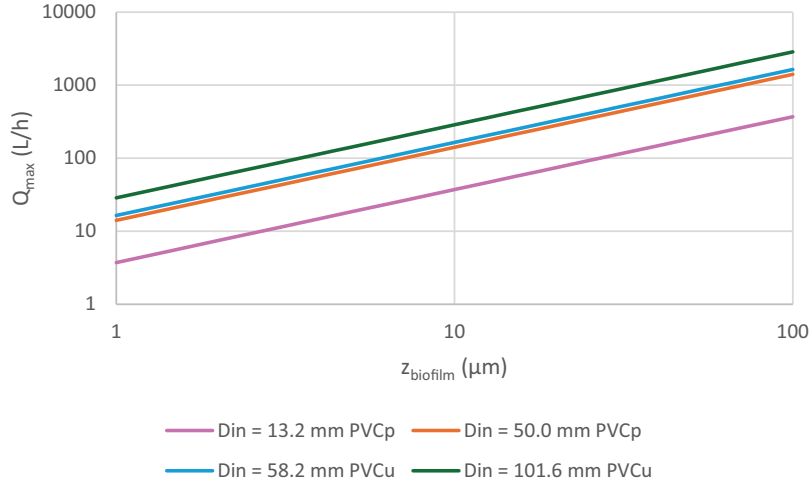

Figure 5. Maximum flow rate required to record Δt_{res} of 2 s for different D_{in} and L_{pipe} = 50 m.

biofouling. For instance, at D_{in} = 58.2 mm, a biofilm 50 µm thick increases the residence time Δt_{res} = 2 s for flow rates $Q \leq 0.8$ m^3/h. Similarly, even for larger pipes with D_{in} = 101.6 mm, a similar change in residence time is observed for flow rates $Q \leq 1.4$ m^3/h.

In real life though, pipe lengths are even greater, and water utilities require measuring thin, e.g. 15 µm, biofilms at different pipe diameters. For this reason, we calculate the minimum biofilm thickness $z_{biofilm,min}$ that can induce a residence time deviation of Δt_{res} = 2 s for different pipe diameters D_{in} and pipe lengths L_{pipe}, as is shown in Figure 6:

Figure 6 shows that for larger pipe diameters (D_{in}) and lengths (L_{pipe}) than those in 'Slimer' (13.2 mm, 50 m), a residence time deviation Δt_{res} = 2 s caused by a thin biofilm layer can still be detected. For L_{pipe} = 1000 m, biofilm thicknesses as low as 10 µm are measurable across all pipe sizes. However, with the largest diameter (D_{in} = 101.6 mm) and a 100 m resolution, at least 100 µm thickness is needed to yield the same Δt_{res}. This highlights the trade-off between detectable biofilm thickness and the density of EC sensors required under realistic DWDS conditions.

The residence time method is more reliable at low flow rates; uncertainty and coefficient of variation increase with higher flows (see Table 3). At 200 L/h (0.36 m/s), the standard deviation of $z_{biofilm}$ nears its mean, reducing precision. Since such velocities are rare outside peak demand, measurements in buried pipes can generally be made with greater confidence during typical operation.

A main limitation of the method is its reliance on comparing biofouled and clean pipe states. In practice, establishing a fully clean baseline is difficult due to

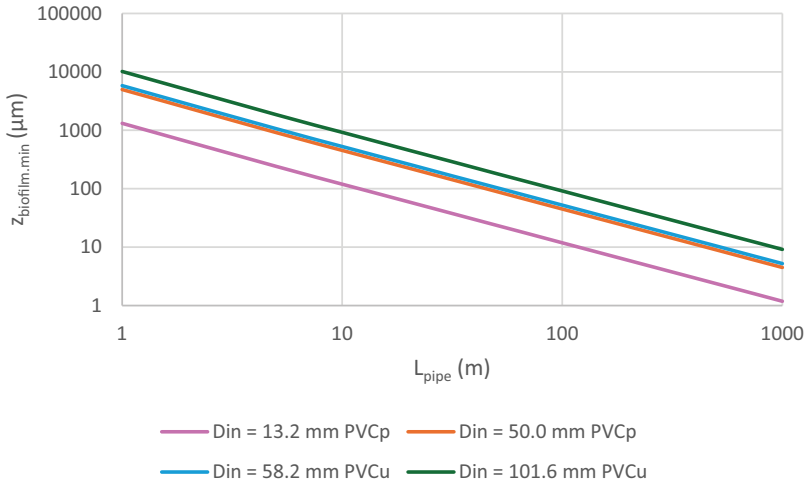

Figure 6. Minimum biofilm thickness $z_{biofilm,min}$ required to record Δt_{res} of 2 s for different D_{in} and u_{mean} = 0.18 m/s.

varying pipe ages and biofilm stages. However, an initial calibration under the cleanest conditions per utility can serve as a reference. As long as infrastructure remains unchanged and sensors remain calibrated, deviations in t_{res} can indicate biofilm growth.

Through hydraulic residence time measurements, we quantified the impact of biofilm growth on flow characteristics, enabling estimates of biofilm thickness. We recognize that the correlation between biofilm accumulation and flow constriction may be influenced by factors such as biofilm morphology and spatial heterogeneity. To strengthen the scientific rigor of these findings, further experimental validation and more detailed characterization of flow dynamics are planned for future work.

4. Conclusions

This study introduces two novel non-intrusive biofilm thickness measurement methods, the heat resistance method and the hydraulic residence time method. Both methods are evaluated within a controlled laboratory setting. The results obtained provide valuable insights into the effectiveness, accuracy and limitations of these approaches, contributing to the ongoing efforts to develop reliable biofilm monitoring tools for drinking water systems. To our knowledge, this is the first study to experimentally compare these two non-intrusive approaches against destructive biovolume validation under realistic pipe-scale hydraulic and thermal conditions.

The heat resistance method, despite its theoretical promise, demonstrated significant measurement variability. This can be attributed to the complex interplay of temperature dynamics, environmental conditions and biofilm heterogeneity, which collectively introduced considerable uncertainty. The method's sensitivity analysis further underscored its dependence on stable and precise thermal measurements, which may limit its applicability in field conditions where environmental variability is inevitable. However, with further refinements, such as improvements in thermal conductivity, modelling and sensor placement, this technique may still offer valuable supplementary data for monitoring additional biofilm characteristics.

Conversely, the hydraulic residence time method exhibited robust and consistent performance, with significantly lower measurement uncertainty. The method's alignment with physical biofilm volume measurements reinforces its potential as a practical monitoring tool. By leveraging subtle changes in flow dynamics induced by biofilm accumulation, this technique enables spatially wide detection of biofilm thickness with minimal infrastructure disruption. The findings suggest that hydraulic residence time analysis could be leveraged to non-destructively measure biofilm thickness in larger and more complex experimental setups, facilitating the development of more realistic biofilm models and enabling water utilities to more effectively manage biofilm-related risks in their networks.

The study's results emphasize the importance of selecting biofilm monitoring techniques based on system-specific conditions and operational constraints. While hydraulic residence time measurements appear promising for broader application, the refinement of heat resistance analysis could further enhance biofilm characterization efforts.

The work prented here was conducted under fully controlled laboratory condifitions designed to simulate key features of real distribution systems. Still, future

research should focus on further testing and validation of the two methods in more realistic DWDS environments, addressing a number of different challenges related to practical implementation such as variations in pipe material, network configuration and flow dynamics. Potential synergies between the two techniques could be explored too.

Ultimately, the development of reliable, non-intrusive biofilm monitoring method will empower water utilities to adopt more proactive and targeted biofilm management strategies, improving both water quality and infrastructure longevity. By integrating advanced sensing technologies into DWDS monitoring practices, the industry can enhance its ability to mitigate biofilm-related risks while minimizing costly and potentially disruptive maintenance interventions.

Acknowledgements

The authors thank Paul van der Wielen (KWR & Radboud University) and Anke Brouwer–Hanzens (KWR) for their support and advice on the microbiological aspects of the research and Robbie van Pelt (KWR) for his technical advice and assistance in realizing and operating the experiments.

Author contributions

CRediT: **Konstantinos Glynis:** Data curation, Formal analysis, Investigation, Methodology, Writing – original draft; **Mirjam Blokker:** Investigation, Methodology, Supervision; **Zoran Kapelan:** Methodology, Supervision; **Dragan Savić:** Methodology, Supervision.

Disclosure statement

No potential conflict of interest was reported by the author(s).

Funding

This work was supported by the "Smart Water Futures" project which has received funding from the European Research Council (ERC) under the European Union's Horizon 2020 research and innovation program, Grant agreement No. [951424].

Data availability statement

Data will be made available on request.

Declaration of generative AI in scientific writing

During the preparation of this work, the authors did not use generative AI tools.

References

Afonso, A. C., M. Simões, M. J. Saavedra, L. Simões, J. M. Lema, and A. Trueba-Santiso. 2024. "Exploring Coaggregation Mechanisms Involved in Biofilm Formation in Drinking Water through a Proteomic-Based Approach." *Journal of Applied Microbiology* 135 (6): lxae143. https://doi.org/10.1093/jambio/lxae143.

Anderson, D. R. 1966. "Thermal Conductivity of Polymers." *Chemical Reviews* 66 (6): 677–690. https://doi.org/10.1021/cr60244a004.

Bakke, R., R. Kommedal, and S. Kalvenes. 2001. "Quantification of Biofilm Accumulation by an Optical Approach." *Journal of Microbiological Methods* 44 (1): 13–26. https://doi.org/10.1016/S0167-7012(00)00236-0.

Calero Preciado, C., S. Husband, J. Boxall, G. Olmo, V. Soria-Carrasco, S. K. Maeng, and I. Douterelo. 2021. "Intermittent Water Supply Impacts on Distribution System Biofilms and Water Quality." *Water Research* 201:117372. https://doi.org/10.1016/j.watres.2021.117372.

Calero Preciado, C., V. Soria-Carrasco, J. Boxall, and I. Douterelo. 2022. "Climate Change and Management of Biofilms Within Drinking Water Distribution Systems." *Frontiers in Environmental Science* 10:10. https://doi.org/10.3389/fenvs.2022.962514.

CEN. 2014. *CEN-EN16421:2014 Influence of Materials on Water for Human Consumption - Enhancement of Microbial Growth*. Brussels: European Committee for Standardization (CEN).

Çengel, Y. A. 2002. *Heat Transfer: A Practical Approach*. 2nd ed. New York, NY, USA: McGraw-Hill.

Çengel, Y. A., and A. J. Ghajar. 2015. *Heat and Mass Transfer: Fundamentals & Applications*. 5th ed. New York, NY, USA: McGraw-Hill.

Chen, X., S. R. Suwarno, T. H. Chong, D. McDougald, S. Kjelleberg, Y. Cohen, A. G. Fane, and S. A. Rice. 2013. "Dynamics of Biofilm Formation Under Different Nutrient Levels and the Effect on Biofouling of a Reverse Osmosis Membrane System." *Biofouling* 29 (3): 319–330. https://doi.org/10.1080/08927014.2013.772141.

Delpla, I., A.-V. Jung, E. Baures, M. Clement, and O. Thomas. 2009. "Impacts of Climate Change on Surface Water Quality in Relation to Drinking Water Production." *Environment International* 35 (8): 1225–1233. https://doi.org/10.1016/j.envint.2009.07.001.

dos Santos, L. M. F., and A. G. Livingston. 1995. "Membrane-Attached Biofilms for VOC Wastewater Treatment I: Novel in situ Biofilm Thickness Measurement Technique." *Biotechnology and Bioengineering* 47 (1): 82–89. https://doi.org/10.1002/bit.260470110.

Douterelo, I., S. Husband, V. Loza, and J. Boxall. 2016. "Dynamics of Biofilm Regrowth in Drinking Water Distribution Systems." *Applied and Environmental Microbiology* 82 (14): 4155–4168. https://doi.org/10.1128/AEM.00109-16.

Dreszer, C., J. S. Vrouwenvelder, A. H. Paulitsch-Fuchs, A. Zwijnenburg, J. C. Kruithof, and H.-C. Flemming. 2013. "Hydraulic Resistance of Biofilms." *Journal of Membrane Science* 429:436–447. https://doi.org/10.1016/j.memsci.2012.11.030.

Fass, S., J. C. Block, M. Boualam, V. Gauthier, D. Gatel, J. Cavard, S. Benabdallah, and V. Lahoussine. 2003. "Release of Organic Matter in a Discontinuously Chlorinated Drinking Water

Network." *Water Research* 37 (3): 493–500. https://doi.org/10.1016/S0043-1354(02)00362-7.

Fish, K., A. M. Osborn, and J. B. Boxall. 2017. "Biofilm Structures (EPS and Bacterial Communities) in Drinking Water Distribution Systems Are Conditioned by Hydraulics and Influence Discolouration." *Science of the Total Environment* 593-594:571–580. https://doi.org/10.1016/j.scitotenv.2017.03.176.

Flemming, H.-C., S. L. Percival, and J. T. Walker. 2002. "Contamination Potential of Biofilms in Water Distribution Systems." *Water Supply* 2 (1): 271–280. https://doi.org/10.2166/ws.2002.0032.

Flemming, H.-C., and J. Wingender. 2010. "The Biofilm Matrix." *Nature Reviews Microbiology* 8 (9): 623–633. https://doi.org/10.1038/nrmicro2415.

Flemming, H.-C., J. Wingender, U. Szewzyk, P. Steinberg, S. A. Rice, and S. Kjelleberg. 2016. "Biofilms: An Emergent Form of Bacterial Life." *Nature Reviews Microbiology* 14 (9): 563–575. https://doi.org/10.1038/nrmicro.2016.94.

Glynis, K., M. Blokker, Z. Kapelan, and D. Savić. 2024. "Experimental Setup for Measuring the Effect of Biofilm Build-Up on Heat Transfer in Drinking Water Pipes." *Engineering Proceedings* 69:169. https://doi.org/10.3390/engproc2024069169.

Gomes, I. B., M. Simões, and L. C. Simões. 2014. "An Overview on the Reactors to Study Drinking Water Biofilms." *Water Research* 62:63–87. https://doi.org/10.1016/j.watres.2014.05.039.

Henne, K., L. Kahlisch, I. Brettar, and M. G. Höfle. 2012. "Analysis of Structure and Composition of Bacterial Core Communities in Mature Drinking Water Biofilms and Bulk Water of a Citywide Network in Germany." *Applied and Environmental Microbiology* 78 (10): 3530–3538. https://doi.org/10.1128/AEM.06373-11.

Husband, P. S., and J. B. Boxall. 2011. "Asset Deterioration and Discolouration in Water Distribution Systems." *Water Research* 45 (1): 113–124. https://doi.org/10.1016/j.watres.2010.08.021.

Husband, S., K. E. Fish, I. Douterelo, and J. Boxall. 2016. "Linking Discolouration Modelling and Biofilm Behaviour Within Drinking Water Distribution Systems." *Water Supply* 16 (4): 942–950. https://doi.org/10.2166/ws.2016.045.

Jungfer, C., F. Friedrich, J. Varela Villarreal, K. Brändle, H.-J. Gross, U. Obst, and T. Schwartz. 2013. "Drinking Water Biofilms on Copper and Stainless Steel Exhibit Specific Molecular Responses Towards Different Disinfection Regimes at Waterworks." *Biofouling* 29 (8): 891–907. https://doi.org/10.1080/08927014.2013.813936.

Kalmbach, S., W. Manz, and U. Szewzyk. 1997. "Isolation of New Bacterial Species from Drinking Water Biofilms and Proof of Their in Situ Dominance with Highly Specific 16S rRNA Probes." *Applied and Environmental Microbiology* 63 (11): 4164–4170. https://doi.org/10.1128/aem.63.11.4164-4170.1997.

Learbuch, K. L. G., H. Smidt, and P. W. J. J. Wielen. 2021. "Influence of Pipe Materials on the Microbial Community in Unchlorinated Drinking Water and Biofilm." *Water Research* 194:116922. https://doi.org/10.1016/j.watres.2021.116922.

Lehtola, M. J., I. T. Miettinen, M. M. Keinänen, T. K. Kekki, O. Laine, A. Hirvonen, T. Vartiainen, and P. J. Martikainen. 2004. "Microbiology, Chemistry and Biofilm Development in a Pilot Drinking Water Distribution System with Copper and Plastic Pipes." *Water Research* 38 (17): 3769–3779. https://doi.org/10.1016/j.watres.2004.06.024.

Li, Z., R. M. Clark, S. G. Buchberger, and Y. Jeffrey Yang. 2014. "Evaluation of Climate Change Impact on Drinking Water Treatment Plant Operation." *Journal of Environmental Engineering* 140 (9): A4014005. https://doi.org/10.1061/(ASCE)EE.1943-7870.0000824.

Liu, J., R. Martinez-Corral, A. Prindle, D. D. Lee, J. Larkin, M. Gabalda-Sagarra, J. Garcia-Ojalvo, and G. M. Süel. 2017. "Coupling Between Distant Biofilms and Emergence of Nutrient Time-Sharing." *Science* 356 (6338): 638–642. https://doi.org/10.1126/science.aah4204.

Liu, S., C. Gunawan, N. Barraud, S. A. Rice, E. J. Harry, and R. Amal. 2016. "Understanding, Monitoring, and Controlling Biofilm Growth in Drinking Water Distribution Systems." *Environmental Science & Technology* 50 (17): 8954–8976. https://doi.org/10.1021/acs.est.6b00835.

Mathieu, L., I. Bertrand, Y. Abe, E. Angel, J. C. Block, S. Skali-Lami, and G. Francius. 2014. "Drinking Water Biofilm Cohesiveness Changes Under Chlorination or Hydrodynamic Stress." *Water Research* 55:175–184. https://doi.org/10.1016/j.watres.2014.01.054.

Maurício, R., C. J. Dias, N. Jubilado, and F. Santana. 2013. "Biofilm Thickness Measurement Using an Ultrasound Method in a Liquid Phase." *Environmental Monitoring and Assessment* 185 (10): 8125–8133. https://doi.org/10.1007/s10661-013-3160-0.

Moreno, Y., L. Moreno-Mesonero, P. Soler, A. Zornoza, and A. Soriano. 2024. "Influence of Drinking Water Biofilm Microbiome on Water Quality: Insights from a Real-Scale Distribution System." *Science of the Total Environment* 921:171086. https://doi.org/10.1016/j.scitotenv.2024.171086.

Neu, L., C. R. Proctor, J.-C. Walser, and F. Hammes. 2019. "Small-Scale Heterogeneity in Drinking Water Biofilms." *Frontiers in Microbiology* 10. https://doi.org/10.3389/fmicb.2019.02446.

Paquin, J., J. Block, K. Haudidier, P. Hartemann, F. Colin, J. Miazga, and Y. Levi. 1992. "Effect of Chlorine on the Bacterial Colonisation of a Model Distribution System." *Revue Des Sciences De L'Eau* 5 (3): 399–414. https://doi.org/10.7202/705138ar.

Prest, E. I., F. Hammes, M. C. M. Loosdrecht, and J. S. Vrouwenvelder. 2016. "Biological Stability of Drinking Water: Controlling Factors, Methods, and Challenges." *Frontiers in Microbiology* 7. https://doi.org/10.3389/fmicb.2016.00045.

Revetta, R. P., A. Pemberton, R. Lamendella, B. Iker, and J. W. Santo Domingo. 2010. "Identification of Bacterial Populations in Drinking Water Using 16S rRNA-Based Sequence Analyses." *Water Research* 44 (5): 1353–1360. https://doi.org/10.1016/j.watres.2009.11.008.

Schwering, M., J. Song, M. Louie, R. J. Turner, and H. Ceri. 2013. "Multi-Species Biofilms Defined from Drinking Water Microorganisms Provide Increased Protection Against Chlorine Disinfection." *Biofouling* 29 (8): 917–928. https://doi.org/10.1080/08927014.2013.816298.

Seneviratne, C. J., Y. Wang, L. Jin, S. S. W. Wong, T. D. K. Herath, and L. P. Samaranayake. 2012. "Unraveling the Resistance of Microbial Biofilms: Has Proteomics Been Helpful?" *Proteomics* 12 (4–5): 651–665. https://doi.org/10.1002/pmic.201100356.

Shen, Y., C. Huang, G. L. Monroy, D. Janjaroen, N. Derlon, J. Lin, R. Espinosa-Marzal, et al. 2016. "Response of Simulated

Drinking Water Biofilm Mechanical and Structural Properties to Long-Term Disinfectant Exposure." *Environmental Science & Technology* 50 (4): 1779–1787. https://doi.org/10.1021/acs.est.5b04653.

Shen, Y., G. L. Monroy, N. Derlon, D. Janjaroen, C. Huang, E. Morgenroth, S. A. Boppart, N. J. Ashbolt, W.-T. Liu, and T. H. Nguyen. 2015. "Role of Biofilm Roughness and Hydrodynamic Conditions in Legionella pneumophila Adhesion to and Detachment from Simulated Drinking Water Biofilms." *Environmental Science & Technology* 49 (7): 4274–4282. https://doi.org/10.1021/es505842v.

Singer, P. C. 1994. "Control of Disinfection By-Products in Drinking Water." *Journal of Environmental Engineering* 120 (4): 727–744. https://doi.org/10.1061/(ASCE)0733-9372(1994)120:4(727).

Tsagkari, E., S. Connelly, Z. Liu, A. McBride, and W. T. Sloan. 2022. "The Role of Shear Dynamics in Biofilm Formation." *NPJ Biofilms and Microbiomes* 8 (1): 33. https://doi.org/10.1038/s41522-022-00300-4.

Türetgen, I. 2004. "Comparison of the Efficacy of Free Residual Chlorine and Monochloramine Against Biofilms in Model and Full Scale Cooling Towers." *Biofouling* 20 (2): 81–85. https://doi.org/10.1080/08927010410001710027.

van der Kooij, D., J. Hein, M. van Lieverloo, J. Schellart, and P. Hiemstra. 1999. "Maintaining Quality Without a Disinfectant Residual." *Journal AWWA* 91 (1): 55–64. https://doi.org/10.1002/j.1551-8833.1999.tb08568.x.

van der Kooij, D., and P. W. J. J. van der Wielen. 2013. *Microbial Growth in Drinking-Water Supplies: Problems, Causes, Control and Research Needs*. London, UK: IWA Publishing.

van der Wielen, P. W. J. J., M. Dignum, A. Donocik, and E. I. Prest. 2023. "Influence of Temperature on Growth of Four Different Opportunistic Pathogens in Drinking Water Biofilms." *Microorganisms* 11 (6): 1574. https://doi.org/10.3390/microorganisms11061574.

van der Wielen, P. W. J. J., and D. van der Kooij. 2010. "Effect of Water Composition, Distance and Season on the Adenosine Triphosphate Concentration in Unchlorinated Drinking Water in the Netherlands. Water Research, Microbial Ecology of Drinking Water and Waste Water Treatment Processes." *Water Research* 44 (17): 4860–4867. https://doi.org/10.1016/j.watres.2010.07.016.

Vreeburg, J., M. Blokker, P. Horst, and J. C. van Dijk. 2009. "Velocity-Based Self-Cleaning Residential Drinking Water Distribution Systems." *Water Supply* 9 (6): 635–641. https://doi.org/10.2166/ws.2009.689.

Wagner, M., and H. Horn. 2017. "Optical Coherence Tomography in Biofilm Research: A Comprehensive Review." *Biotechnology and Bioengineering* 114 (7): 1386–1402. https://doi.org/10.1002/bit.26283.

Zhao, Z., Y.-H. Luo, T.-H. Wang, S. Sinha, L. Ling, B. Rittmann, P. Alvarez, F. Perreault, and P. Westerhoff. 2023. "Phenotypic and Transcriptional Responses of Pseudomonas Aeruginosa Biofilms to UV-C Irradiation via Side-Emitting Optical Fibers: Implications for Biofouling Control." *Environmental Science & Technology* 57 (41): 15736–15746. https://doi.org/10.1021/acs.est.3c04658.

Zlatanovic, L., A. Moerman, J. P. van der Hoek, J. Vreeburg, and M. Blokker. 2017. "Development and Validation of a Drinking Water Temperature Model in Domestic Drinking Water Supply Systems." *Urban Water Journal* 14 (10): 1031–1037. https://doi.org/10.1080/1573062X.2017.1325501.

Appendices

Appendix A. Water physio-chemistry

The water used in the experiments was standard tap water supplied by Vitens N.V., the largest water utility in the Netherlands, serving the Nieuwegein area. This water originates from groundwater aquifers and undergoes extensive treatment to remove most organic compounds, ensuring high biological stability. Due to its underground source, the water's physico-chemical properties show minimal, if any, variation. Nevertheless, rigorous and regular testing is conducted by Vitens Waterexpertisecentrum, the utility's water quality division. The key physico-chemical parameters of the water reaffirming the biological stability are:

Despite the biological stability of the provided water, biofilm was able to grow relatively rapidly in the 'Slimer' setup thanks mainly to the high plasticizer content of the pipe material used, i.e. PVCp.

Table A1. Physio-chemical properties of water.

	Range		
Parameter	Min	Max	Units
Oxygen	10.2	10.9	mg/l
Turbidity	<0.1	0.28	FTE
EC	23.3	25.0	mS/m
TOC	1.6	1.6	mg/l
Ammonium	<0.03	<0.03	mg/l
Nitrate	<1.0	<1.0	mg/l
Nitrite	<0.01	<0.01	mg/l
Total hardness	1.09	1.24	mmol/l

Appendix B. Estimation of the external heat resistance

In the Slimer setup, the fan installed at the base of the helical pipe pushes air at a speed u_{air} of approximately 1.5 m/s. For D_{out} of 19.8 mm and a kinematic viscosity v_{air} of air at 25°C equal to $1.562{\cdot}10^{-5}$ m^2/s (Çengel and Ghajar 2015) we get an air flow Reynolds number equal to:

$$Re_{air} = \frac{u_{air} \cdot D_{out}}{v_{air}} = \frac{1.5 \cdot 0.0198}{1.562 \cdot 10^{-5}} = 1,901 \tag{B.1}$$

By using the empirical value of Prandtl number Pr of 0.730 for air at 25°C (Çengel and Ghajar 2015), we then calculate the Nusselt number Nu_{air} of the air flow using the empirical correlation for forced convection over circular cylinders in cross flow when $Re \in (40, 4000)$ (Çengel 2002):

$$Nu_{air} = 0.683 \cdot Re^{0.466} \cdot Pr^{0.333} = 0.683 \cdot 1,901^{0.466} \cdot 0.730^{0.333} = 20.75 \tag{B.2}$$

Thus, according to Eq. (8), and considering the thermal capacity of air k_{air} at 25°C to be 0.026 W/m/°C (Çengel and Ghajar 2015), the external heat resistance is calculated to be:

$$R_{ext} = \frac{1}{\pi \cdot 50 \cdot 0.026 \cdot 20.75} = 0.0118°C/W \tag{B.3}$$

To assess whether this value is realistic, we compare the R_{ext} value of (S.M.3) to the one the subtraction of R_{int} and R_{pipe} from R_{total} yield in experimental conditions. As is described below in section S.M.4, for $Q = 200$ l/h in biofouled conditions we measure $T_{in} =$ 13.28°C, $T_{out} = 15.81$°C, $I = 26.87$°C. By plugging these values into Eqs. (4), (6), and (7) and solving for I, we get $x = 0.0120$ °C/W. This calculated value of the external heat resistance is almost identical to the one calculated as the remainder of the sum of all the other components of heat resistance. This is reasonable considering this calculation neglects minor alterations caused by the setup structure, including any shielding effect each loop has on the adjacent ones.

Appendix C. Derivation of biofilm thickness from residence time measurements

To compare residence times with and without biofilm, the flow rate remains constant among those two instances. Hence, the flow rate in the clean pipe Q_{clean} and the flow rate in the biofouled pipe $Q_{biofilm}$ are equal $Q_{clean} = Q_{biofilm}$.

For a constant flow rate then, the growth of biofilm causes the available cross section of the pipe to be reduced from $\frac{\pi}{4} \cdot {D_{in}}^2$ to a smaller area equal to $\frac{\pi}{4} \cdot (D_{in} - 2z_{biofilm})^2$. Knowing that the flow rate remained constant, it holds that:

$$\frac{\frac{\pi}{4}\cdot {D_{in}}^2}{t_{res,clean}} = \frac{\frac{\pi}{4}\cdot (D_{in}-2z_{biofilm})^2}{t_{res,biofilm}} \tag{C.1}$$

Solving Eq. (C.1) for $z_{biofilm}$, yields Eq. (11).

Appendix D. Detailed Sensitivity Calculations

As for the heat resistance method sensitivity, since $R_{biofilm}$ is defined as the alteration of R_{total} over time, we investigate the sensitivity of the latter with respect to the measured parameters. Let the measurement uncertainties be: σ_m, $\sigma_{T_{in}}$, $\sigma_{T_{out}}$, and $\sigma_{T_{air}}$ for m, T_{in}, T_{out}, and T_{air}, respectively. To perform the uncertainty propagation, we use the partial derivative method and compute the partial derivatives of R_{total} with respect to each variable. The partial differentials for m, T_{in}, T_{out}, and T_{air} are provided here:

$$\frac{\partial R_{total}}{\partial m} = \frac{1}{m^2 C_{p,water} ln\left(\frac{T_{air}-T_{out}}{T_{air}-T_{in}}\right)} \tag{D.1}$$

$$\frac{\partial R_{total}}{\partial T_{in}} = \frac{1}{mC_{p,water}}\cdot\frac{1}{T_{air}-T_{in}} \tag{D.2}$$

$$\frac{\partial R_{total}}{\partial T_{out}} = \frac{1}{mC_{p,water}}\cdot\frac{1}{T_{air}-T_{out}} \tag{D.3}$$

$$\frac{\partial R_{total}}{\partial T_{air}} = \frac{1}{mC_{p,water}}\cdot\left(\frac{1}{T_{air}-T_{out}}-\frac{1}{T_{air}-T_{in}}\right) \tag{D.4}$$

To compare these derivatives, we substitute the parameters with typical values measured during the experiment. A comprehensive overview of the measured parameters across all flow rates in both biofouled and clean conditions can be found in Appendix E. Here, we focus on the biofouled conditions observed on 16 December 2024, for all four flow rates. The calculations for the highest flow rate, 200 L/h, are presented below.

A measured flow rate Q equal to 200 l/h translates to a mass flux of $55.5{\cdot}10^{-3}$ kg/s. The measured T_{in}, T_{out}, and T_{air} are equal to 13.28°C, 15.81°C, and 26.87°C, respectively. By replacing these values in Eqs. (D.1)–(D.4), we calculate the partial differentials: $\frac{\partial R_{total}}{\partial m} = -3.8\cdot 10^{-1}\,\frac{°C\cdot s^2}{kg\cdot J}$, $\frac{\partial R_{total}}{\partial T_{in}} = 3.2\cdot 10^{-4}\,\frac{s}{J}$, $\frac{\partial R_{total}}{\partial T_{out}} = 3.9\cdot 10^{-4}\,\frac{s}{J}$, $\frac{\partial R_{total}}{\partial T_{air}} = 7.3\cdot 10^{-5}\,\frac{s}{J}$.

The uncertainty in R_{total}, denoted as $\sigma_{R_{total}}$ is given by the root-sum-square of the individual uncertainties propagated through the partial derivatives as follows:

$$\sigma_{R_{total}} = \sqrt{\left(\frac{\partial R_{total}}{\partial m}\cdot\sigma_m\right)^2+\left(\frac{\partial R_{total}}{\partial T_{in}}\cdot\sigma_{T_{in}}\right)^2+\left(\frac{\partial R_{total}}{\partial T_{out}}\cdot\sigma_{T_{out}}\right)^2+\left(\frac{\partial R_{total}}{\partial T_{air}}\cdot\sigma_{T_{air}}\right)^2} \tag{D.5}$$

The mass flux is a product of ρ_{water} and Q. Thus, the mass flux uncertainty σ_m depends on the flow rate uncertainty σ_Q as follows:

$$\sigma_m = \rho_{water}\cdot\sigma_Q \tag{D.6}$$

The technical characteristics of the sensors and/or the calibration performed (see Appendix F for more details) provide the measurement uncertainties. The flow rate uncertainty is $\sigma_Q = \pm 1.13 l/h$, hence the mass flux uncertainty is $\sigma_m = 3.14\cdot 10^{-4}\,\frac{kg}{s}$. The temperature uncertainty is $\sigma_{T_{in}} = \sigma_{T_{out}} = \sigma_{T_{air}} = 0.15°C + 0.002T$, where T is the corresponding temperature. For the water and air temperature, we get $\sigma_{T_{in}} = 0.177$, $\sigma_{T_{out}} = 0.182$, and $\sigma_{T_{air}} = 0.204$. By plugging these values into the squared terms within the squared root of Eq. (D.5), we get: $\left|\frac{\partial R_{total}}{\partial m}\cdot\sigma_m\right| = 1.18\cdot 10^{-4}\,\overline{W}$, $\left|\frac{\partial R_{total}}{\partial T_{in}}\cdot\sigma_{T_{in}}\right| = 0.56\cdot 10^{-4}\,\overline{W}$, $\left|\frac{\partial R_{total}}{\partial T_{out}}\cdot\sigma_{T_{out}}\right| = 0.71\cdot 10^{-4}\,\overline{W}$, and $\left|\frac{\partial R_{total}}{\partial T_{air}}\cdot\sigma_{T_{air}}\right| = 0.15\cdot 10^{-4}\,\overline{W}$. From the balance between these different terms, we see that 45% of the total variability stems from the mass flux uncertainty. The total heat resistance uncertainty is $\sigma_{R_{total}} = 1.49\cdot 10^{-4}\,\overline{W}$.

Taking into account that temporal changes of R_{total} are expressed as $R_{biofilm}$, the sensitivity of $z_{biofilm}$ is given by the product of $\sigma_{R_{total}}$ and $\frac{\partial z_{biofilm}}{\partial R_{total}}$, where $\frac{\partial z_{biofilm}}{\partial R_{total}} = \pi\cdot D_{in}\cdot L_{pipe}\cdot k_{water}$. We therefore calculate a biofilm thickness uncertainty of $\sigma_{z_{biofilm}} = 179$ µm. Repeating these calculations for lower flow rates, we get: $\sigma_{z_{biofilm}} = 247$ µm for 150 l/h, $\sigma_{z_{biofilm}} = 394$ µm and $\sigma_{z_{biofilm}} = 962$ µm.

The high uncertainty of the heat resistance method, particularly for expected biofilm thickness in drinking water pipes, raises concerns about its sensitivity. However, per Eqs. (D.1)–(D.5), increasing flow rate Q raises mass flow m, which appears in the denominator of the partial differentials, thus reducing $\sigma_{R_{total}}$. To maintain adequate residence time, and the resulting temperature difference between T_{in} and T_{out}, longer pipe sections are needed. For example, quadrupling both flow rate and pipe length keeps t_{res} constant while reducing biofilm thickness uncertainty to $\sigma_{z_{biofilm}} = 110$ µm.

Regarding the hydraulic residence time method, the uncertainty in $z_{biofilm}$ depends on the sensitivity of $t_{res,clean}$ and $t_{res,biofilm}$ under clean and biofouled conditions. These, in turn, depend on the standard deviation of the time metrics $t_{i,j}$ (where $i = 1, 2$ and $j = 1, 2, 3$) used in their calculation.

We determine $\sigma_{t_{res,clean}}$ and $\sigma_{t_{res,biofilm}}$ from the experimental standard deviation among the three residence time definitions $t_{res,j}$, $j = 1, 2, 3$. At the highest flow rate (200 l/h) under biofouled conditions, we measure $t_{res,1} = 135.4$ s, $t_{res,2} = 135.5$ s, $t_{res,3} = 135.9$ s, yielding a mean $t_{res,biofilm} = 135.6$ s and $\sigma_{t_{res,biofilm}} = 0.3$ s. Similarly, for clean conditions, $\sigma_{t_{res,clean}} = 0.5$ s.

To compute $\sigma_{z_{biofilm}}$, we apply error propagation from Eq. (D.1): it equals the square root of the sum of squared products between the partial derivatives of $z_{biofilm}$ with respect to residence times and their standard deviations. After simplification, $\sigma_{z_{biofilm}}$ is obtained as:

$$\sigma_{z_{biofilm}} = \frac{D_{in}}{4}\sqrt{\frac{{\sigma_{t_{res,biofilm}}}^2}{t_{res,biofilm}\cdot t_{res,clean}} + \frac{t_{res,biofilm}\cdot {\sigma_{t_{res,clean}}}^2}{{t_{res,clean}}^3}} \tag{D.7}$$

By substituting the previously calculated residence time values and their respective standard deviations, we obtain a sensitivity of $\sigma_{z_{biofilm}} = 14$ µm. This sensitivity is an order of magnitude lower than that of the heat resistance method. The primary reason for this difference is the fewer and more stable influencing parameters in these measurements, specifically the diffusion of the tracer and the electrical conductivity of water, as opposed to temperature variations.

Appendix E. Measured parameters

In Table E1 we provide an overview of the parameters measured using the sensors installed in Slimer.

To improve the measurement accuracy of the flow meters, we performed a volumetric calibration for flow rates between 30 and 200 l/h. At five different equidistant to each other flow rates, we measured the flow multiple times.

Table E1. Measured values of key parameters. Data obtained from this study.

Conditions	Q (l/h)	T_{in} (°C)	T_{out} (°C)	T_{air} (°C)
Biofouled	200	13.28	15.81	26.87
	150	13.31	16.51	26.85
	100	13.32	17.76	26.92
	50	12.56	20.22	26.63
Clean	200	13.00	15.63	27.18
	150	13.20	16.45	26.96
	100	13.46	17.90	26.92
	50	13.31	20.86	26.99

Appendix F. Flow meter calibration

To improve the measurement accuracy of the flow meters, we performed a volumetric calibration for flow rates between 30 and 200 l/h. At five different equidistant to each other flow rates, we measured multiple times the flow rate volumetrically using a beaker. The volumetric measurement took place by collecting the outflowing water within a time span of 60 seconds. If F_{meter}(ml/min), $\overline{F_{ref}}$ (ml/min), and $\sigma_{F_{ref}}$ (ml/min) are the meter readings, the average and standard deviation of the reference (measured) flow rate, respectively, then we get the results presented in Table F1:

Due to the linear nature of the deviations ($F_{meter} - \overline{F_{ref}}$), we perform a linear fit. With $\overline{F_{ref}}$ as the true reference value and F_{meter} as the uncorrected reading we generate a function in the form: $F_{corrected} = a \cdot F_{meter} + b$. From a basic optimization, we calculate the values of the slope and intercept to be: $a = 0.9779$ and $b = -8.7694$ (both in ml/min).

To validate the calibration, we perform a posterior residual analysis. We calculate the new residuals for each calibration point based on the calibrated flow rates $F_{corrected} - \overline{F_{ref}}$, as is presented in Table F2:

As Table F.2 shows, the calibration residuals seem to cluster around 0 with no obvious trend, hence the calibration is valid.

To quantify the total flow measurement uncertainty, after the calibration, we combine three uncertainties: the uncertainty of the flow meter readings $\sigma_{F_{ref}}$, the uncertainty of the fit σ_{fit}, and the uncertainty of the reference device $\sigma_{ref,device}$ with

Table F1. Reference and flow meter readings.

F_{meter}	$\overline{F_{ref}}$	$\sigma_{F_{ref}}$	$F_{meter} - \overline{F_{ref}}$
500	478	2	22
1330	1292	6	38
2160	2108	2	52
2750	2682	18	68
3330	3244	12	86

Table F2. Calibration residuals.

F_{meter}	$F_{corrected}$	$\overline{F_{ref}}$	$F_{corrected} - \overline{F_{ref}}$
500	480	478	2
1330	1292	1292	0
2160	2104	2108	−4
2750	2681	2682	−1
3330	3248	3244	4

which the water volume was measured. These three uncertainties are combined as the root-mean squared sum, as is given here:

$$\Delta Q = \pm\sqrt{\sigma_{F_{ref}}^2 + \sigma_{fit}^2 + \sigma_{ref,device}^2} \tag{F.1}$$

For the flow rate range of interest, we use the highest $\sigma_{F_{ref}}$ equal to 18 ml/min. As for σ_{fit}, we calculate this residual standard deviation from our regression analysis to be equal to 3 ml/min. Lastly, the standard deviation of the reference device is equal to 5 g., which in our specific case of flow meter measurements translates to 5 ml/min. By plugging these values to Eq. (E.1), we compute the total measurement uncertainty $\Delta Q = 18.9$ ml/min, which translates to $\Delta Q = \pm 1.13$ l/h.

Appendix G: Example of Biofilm Coverage in the Experimental Setup

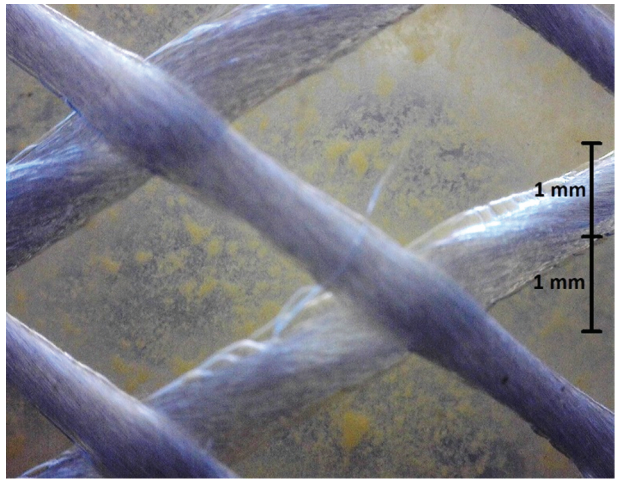

Figure G1. Representative photograph of biofilm coverage inside the PVPp pipe prior to detachment. The biofilm shows relatively uniform distribution, supporting the pipe-averaged assumptions used in the biovolume analysis.

The following Figure G1 provides a representative example of the biofilm coverage observed in the pipe prior to removal. It illustrates the relatively uniform distribution of biomass along the pipe wall during the experimental campaign.